

Accepted Manuscript

Simultaneous measurement of electrostatic charge and its effect on particle motions by electrostatic sensors array in gas-solid fluidized beds

Qiang Shi, Qing Zhang, Guodong Han, Wenbiao Zhang, Jingdai Wang, Zhengliang Huang, Yao Yang, Yongrong Yang, Wenqing Wu, Yong Yan

PII: S0032-5910(17)30142-0
DOI: doi:[10.1016/j.powtec.2017.02.014](https://doi.org/10.1016/j.powtec.2017.02.014)
Reference: PTEC 12352

To appear in: *Powder Technology*

Received date: 19 September 2016
Revised date: 6 January 2017
Accepted date: 9 February 2017



Please cite this article as: Qiang Shi, Qing Zhang, Guodong Han, Wenbiao Zhang, Jingdai Wang, Zhengliang Huang, Yao Yang, Yongrong Yang, Wenqing Wu, Yong Yan, Simultaneous measurement of electrostatic charge and its effect on particle motions by electrostatic sensors array in gas-solid fluidized beds, *Powder Technology* (2017), doi:[10.1016/j.powtec.2017.02.014](https://doi.org/10.1016/j.powtec.2017.02.014)

This is a PDF file of an unedited manuscript that has been accepted for publication. As a service to our customers we are providing this early version of the manuscript. The manuscript will undergo copyediting, typesetting, and review of the resulting proof before it is published in its final form. Please note that during the production process errors may be discovered which could affect the content, and all legal disclaimers that apply to the journal pertain.

Simultaneous measurement of electrostatic charge and its effect on particle motions by electrostatic sensors array in gas-solid fluidized beds

**Qiang Shi^a, Qing Zhang^b, Guodong Han^c, Wenbiao Zhang^d, Jingdai Wang^{a,*},
Zhengliang Huang^a, Yao Yang^a, Yongrong Yang^a, Wenqing Wu^c, Yong Yan^{d,e}**

^a *State Key Laboratory of Chemical Engineering and Department of Chemical and Biological Engineering, Zhejiang University, Hangzhou 310027, P. R. China*

^b *Patent Examination Cooperation Hubei Center of the Patent Office, SIPO, Wuhan 430205, P. R. China*

^c *SINOPEC Tianjin Company, Tianjin 300271, P. R. China*

^d *School of Control and Computer Engineering, North China Electric Power University, Beijing, 102206, China*

^e *School of Engineering and Digital Arts, University of Kent, Canterbury, Kent CT2 7NT, U.K.*

* To whom correspondence should be addressed.

Tel.: +86-571-87951227. Fax: +86-571-87951227.

Corresponding Author:

E-mail address: wangjd@zju.edu.cn.

Abstract

Repeated particle-particle and particle-wall collisions and frictions lead to the generation and accumulation of electrostatic charges in the gas-solid fluidized beds. Variations of electrostatic signals are a rich source of information on particle motions and charging, which have rarely been explored and interpreted. To gain a more comprehensive understanding of the induced electrostatic signals in the fluidized beds, an array of arc-shaped induced electrostatic sensors were attached to the outer wall of a fluidized bed. Combined with cross-correlation method, induced electrostatic voltage signals and correlation velocity of particles were measured simultaneously. It was found that electrostatic charges accumulation restrained the particle motions while the average correlation velocity of particles increased with the amount of injecting liquid antistatic agent. Based on the analyses of induced electrostatic signals, the particle correlation velocity, and the particles charge-to-mass ratio under different charging levels, a predictive model of the average particles charge-to-mass ratio was established. Compared with the results obtained from Faraday cup, the estimated results showed a relative error no more than 40%. Simultaneous measurement of particle correlation velocity and particles charge-to-mass ratio were complemented by arc-shaped induced electrostatic sensors array combined with cross-correlation method.

Keywords: Induced electrostatic voltage; correlation velocity; particle charge-to-mass ratio; liquid antistatic agent

1. Introduction

Gas-solid fluidized beds are widely applied in numerous industrial processes, such as coal combustion and gasification, drying, olefin polymerization and so on. The bubble flow created by injecting gas via a perforated or porous distributor leads to vigorous motions and circulations of solid particles inside the fluidized beds [1,2]. As a result, generation of electrostatic charge in dielectric particles is almost unavoidable due to repeated particle-particle and particle-wall contacts and frictions [3-5]. The generation and variation of electrostatic charge signals are significantly affected by particle motions in the fluidized beds. [6-9] In turn, electrostatic charge accumulation also has a great effect on bubble and particle motions [5,10-13]. Although the measurement of particles charge-to-mass ratio on fluidized particles can assist online process monitoring and control of electrostatic charging levels inside the fluidized bed, reliable, accurate and low-cost method is lacking.

So far, two general methods have been mainly used to measure electrostatic charges in the fluidized beds, namely, the collision electrostatic probe and Faraday cup. Collision electrostatic probes can be used to the online monitoring of electrostatic voltage, potential or current in the fluidized beds [14-16], which indicates the charging levels relatively. Although the collision probes could complement the online measurement of electrostatic voltage or current, it cannot give the particle charge-to-mass ratios directly and has rarely been employed for measuring particles charge-to-mass ratios in the fluidized beds. He et al. [17-19] made the first attempt to use dual-material or dual-tip collision probes to measure particles charge-to-mass ratio and bubble velocity simultaneously. However, collision probes are intrusive and interfere with the flow to a certain extent. Induced electrostatic sensors are non-intrusive and widely applied in dilute pneumatic conveying pipes for particle velocity and concentration measurement. The dynamic induced electrostatic signals

are affected by particle charging and particle motions [20,21]. If information on particles charge-to-mass ratio and particle velocity could be interpreted and decoupled from induced electrostatic signals, a new and non-intrusive method to simultaneously measure these two parameters can be established and the online measurement of particles charge-to-mass ratio can be fulfilled.

Electrostatic sensors array combined with cross-correlation method has been widely and successfully used to measure particle velocity in dilute pneumatic conveying systems [22-25]. Its application has also expanded to characterize the intensity of particle movements in the fluidized beds [26]. Therefore, information on particle motions can be obtained from electrostatic signals. Yan et al.[22] found that the electrostatic current detected by ring-shaped induced electrostatic sensors was proportional to particle charge density and particle velocity, and the proportion coefficient was related to the size of the pipe and the spatial position of the particle. Chen et al. [27,28] developed a charge induction and transfer model based on the electrostatic signals registered by a ball probe when a single bubble passed the probe in a fluidized bed. Based on the model proposed by Chen et al., He et al.[18,29] regressed the relationship among the induced part of electrostatic signals, particle charge-to-mass ratio and bubble velocity, as shown in Eq. (1),

$$I_{ind} = -0.17q_m u_b^{1.1} \quad (1)$$

where I_{ind} represents the induced electrostatic current, q_m stands for particles charge-to-mass ratio, and u_b represents bubble rise velocity. Based on Eq. (1), the particles charge-to-mass ratio could be estimated and the relative error of the prediction results was within 40%.

From the previous work, it can be inferred that a relationship similar to Eq. (1) existed among the induced electrostatic signals, the bubble or particle velocity, and the particles charge-to-mass ratio. Induced electrostatic signals and particle correlation velocity can be obtained by induced electrostatic sensors array, and particles charge-to-mass ratio can be measured by Faraday cup. Our previous research

has demonstrated that injection of a trace of liquid antistatic agent (LAA) can adjust the electrostatic charges to various levels [11,12]. Therefore, LAA injection was conducted in this work to measure the induced electrostatic signals, the particle correlation velocity, and the particles charge-to-mass ratio under different charging levels.

By installing arc-shaped induced electrostatic sensors array around the outer wall of the fluidized bed, this work investigated the effect of electrostatic charges accumulation on particle motions, especially correlation velocity of particles, by injecting various contents of LAA into the fluidized bed. Based on the induced electrostatic signals, the particle correlation velocity, and the particles charge-to-mass ratio under different charging levels, a predictive model of the average particles charge-to-mass ratio was established to complement the online measurement of particles charge-to-mass ratio. The estimated results were compared with those from Faraday cup to demonstrate the reliability and accuracy of the predictive model.

2. Experimental apparatus and methods

Figure 1 shows the schematic diagram of the experimental apparatus, which consists of fluidization system and measurement system. The fluidized bed is made of a transparent Plexiglas column with an inner diameter of 140 mm and a height of 1000 mm. The thickness of the Plexiglas column is 5 mm. The expanded section at the top has a height of 300 mm and a width of 250 mm. An iron perforated distributor is installed at the bottom of the column with 226 holes and an open area ratio 2.6%, along with a gas mixing chamber. Compressed air pre-dried to a relative humidity of 8-15% and within the temperature range of 20-25 °C is used as the fluidizing gas.

The measurement system is composed of electrostatic sensors, electrostatic signal amplification circuits, a data acquisition card (National Instruments, USB-6212) and a computer. The arc-shaped electrostatic sensor is made of copper with a width of 6 mm and a thickness of 2 mm. The central angle of the sensor is 60 degree. The

arc-shaped electrodes were tightly wrapped on the outer wall of the fluidized bed. In each set of the electrodes, the distance between the two adjacent electrodes was 25 mm, as shown in Figure 2.

When charged particles come across the sensitivity zone of electrodes, induced electrostatic charges on the electrodes are affected and electrostatic current is generated, which is transformed, filtered and amplified to electrostatic voltage signal by signal amplification circuit. Grounded metal boxes were installed outside the electrodes and circuit boards in order to eliminate external electrical interference and enhance the signal-to-noise ratio. Electrostatic voltage signals from all the electrodes were recorded in a computer through the data acquisition card. The sampling time period was 200 s. The sampling frequency was determined by the maximum particle velocity, distance between adjacent sensors, and the tolerance of standard deviations of the transit time. In this work, the sampling frequency selected was 4000 Hz. By calculating the transit time between electrostatic voltage signals from the adjacent sensors, correlation velocity of particle clouds was obtained [26] and could be used to compare the intensity of particle motions under different electrostatic charge levels. The Faraday cup electrometer (Monroe Electronics, NanoCoulomb Meter 284) was used to measure the average charge-to-mass ratio of charged particles. The sampling ports were set at 90 and 230 mm above the distributor, as shown in Figure 2. The charged particles from sampling port went directly into the Faraday cup due to the pressure difference between inside and outside of the fluidized bed. Considering the possible influence of sampling process on measurements, all experimental runs were repeated at least three times to ensure the reproducibility of the results.

The fluidized particles used in the experiments were linear low density polyethylene (LLDPE) particles and polypropylene (PP) particles, supplied by a branch company of Sinopec. Specific physical properties of the particles and operating parameters are indicated in Table 1. The particle size distribution of the polyethylene particles is shown in Figure 3. The minimum fluidization velocity (u_{mf})

was determined by the conventional pressure drop method [30]. The fluidized bed was operated in the bubbling flow regime in the superficial gas velocity (u) range covered in these experiments. The static height of the bed was kept at 265 mm when different types of particles were used.

In order to investigate the electrostatic effects on particle motions, LAA was injected into the fluidized bed through an injection position close to the distributor to control the electrostatic level. The LAA used in this work was AtmerTM 163, which was the same with our previous work [11, 12]. The mass ratio of LAA was calculated on the basis of the weight of particles, as displayed in Tables 2 and 3, respectively.

The work in this paper consists of two parts. The first part focused on the effect of electrostatic charges on particle motions, especially on the correlation velocity of particle clouds. In this part, the same excess velocity ($u_e = u - u_{mf}$) was used for Geldart B and D particles, but different contents of LAA were injected into the fluidized bed to control the electrostatic charges to various levels. Correlation velocities under different electrostatic levels were measured and compared.

Since the electrostatic charge signals measured in the fluidized bed contains dynamic information on both particle motions and particle charging. Based on the correlation velocity measured under different charging levels, the second part established an online measuring method of average charge-to-mass ratio of Geldart B particles. The average particle charge-to-mass ratios were measured by this online method and offline Faraday cup under different superficial gas velocities to demonstrate the reliability of this method.

3. Results and discussions

3.1 Electrostatic effect on correlation velocity of particle clouds

When particles were charged to a saturate level after fluidization for over 30 min, induced electrostatic voltage signals on the electrostatic sensors were recorded simultaneously for 200 s. Figure 4(a) shows the variation of induced electrostatic

voltage signals with time measured by the sensor at $H=180$ mm at an excess gas velocity of 0.35 m/s. The corresponding power spectral density (PSD) of electrostatic voltage is displayed in Figure 4(b), which is mainly located in the frequency range of 0-5 Hz. When a trace of LAA was injected into the fluidized bed, electrostatic voltage decreased remarkably and then reached a new level of equilibrium after nearly 10 min, as shown in Figure 5.

Figure 6 further shows the axial profiles of average positive electrostatic voltage under different contents of LAA for both Geldart D and B particles. It can be indicated that with the increase of LAA contents, the average positive electrostatic voltage decreased, which means that the average fluctuating amplitude of electrostatic voltage signals became smaller. For Geldart D particles, the average positive electrostatic voltage decreased by nearly 70% when the mass ratio of LAA was 50 ppm. However, for Geldart B particles, the average positive electrostatic voltage only decreased by 24% at the same LAA content. When LAA content increased to 125 ppm, the average electrostatic voltage of Geldart B particles reduced by 70%. This implied that for fluidized particles of different Geldart types, the effect of LAA to reduce the electrostatic charge was distinct. Since LAA has good conductivity for its hydrophilic group (-OH), the surface charge dissipation rate of fluidized particles accelerated after injection of LAA and the fluctuating amplitude of induced electrostatic voltage decreased [11]. Therefore, the surface properties of charged particles would determine the effect of LAA to a certain extent. In this work, the average diameter of PP particles was larger and the degree of sphericity was better than LLDPE particles, which was beneficial to the uniform distribution of LAA on particle surfaces. Consequently, LAA was more effective to PP particles.

Although the decrease of the average positive electrostatic voltage indicated the reduction of electrostatic charges of fluidized particles, the fluctuation of induced electrostatic voltage was affected by both electrostatic charge and velocity of particles. Therefore, to illustrate the change of electrostatic charge level more directly, Figure 7

displays the variations of particle charge-to-mass ratios by Faraday cup with the increasing content of LAA. It was demonstrated that the average charge-to-mass ratios of both Geldart D and B particles decreased with the increase of LAA content and finally reached nearly zero.

After the effective control of electrostatic charge by LAA injection, correlation velocity of particle clouds could be compared under different electrostatic levels. Before calculating the correlation velocity, correlation coefficient between the upstream and downstream electrostatic voltage signals should be provided first. Figure 8 shows the two related induced electrostatic voltage signals measured by upstream and downstream sensors and the corresponding cross-relation function. It is seen that the variations of upstream and downstream induced electrostatic voltage signals were similar. Conclusions can also be drawn from Figure 8(b) where correlation coefficient reached the maximum value of 0.932 with a time interval τ_m of 0.0625 s. In this work, the upstream and downstream induced electrostatic signals were highly similar when the maximum correlation coefficient was greater than 0.6. Figure 9 presents the maximum correlation coefficients with time and the calculated correlation velocity. The average value of maximum correlation coefficients for the induced electrostatic signals was 0.8691. The correlation velocity fluctuated between 0.3342 m/s and 0.6523 m/s. The average value of it was 0.451 m/s as present in Table 4.

In order to investigate whether the electrostatic charge level would affect the correlation coefficient between the upstream and downstream electrostatic voltage signals, the average maximum correlation coefficients under different LAA contents for Geldart D particles at two axial heights, as shown in Figure 10. The heights $H=102.5$ mm and $H=217.5$ mm represented for the first two pairs of electrostatic sensors above the distributor, respectively. It can be found in Figure 10 that the average maximum correlation coefficient remained almost unchanged with increasing LAA content, which means that the correlation velocity calculation are not be affected

by electrostatic charge levels and could be used to characterize the intensity of particle motions.

Figure 11 indicated variations of average correlation velocity of particle clouds with LAA content at two axial heights. For both Geldart D and B particles, the average correlation velocity increased with increasing LAA content. This implied that electrostatic charges accumulation in the fluidized bed restrained particle motions, which was also verified in our previous work [12]. Compared to average correlation velocity when particles were fresh or almost uncharged, the average correlation velocity decreased by 26% and 50%, for Geldart D and B particles when particles were charged to a saturate level, which gives a quantitative indication of the electrostatic effect on particle motions.

Table 4 further displays the average correlation velocities of Geldart D and B particles with and without electrostatic charges under two excess gas velocities. It was demonstrated that electrostatic charge accumulation reduced the intensity of particle motions and the average correlation velocity of particles. Figure 12 further shows the normalized probability distributions of correlation velocities of Geldart D particles at two axial heights. With the decrease of electrostatic level, the distribution broadened and the correlation velocity corresponding to the peak of the distribution increased. In a word, the average correlation velocity and the normalized probability distribution of correlation velocities both indicated that electrostatic charges accumulation inhibited particle movements inside the fluidized bed.

The reduction of the intensity of particle motions due to electrostatic charge accumulation can be explained by the following two aspects. Firstly, in our experimental system, particles were mainly negatively charged and the repulsion force between particles dominated, which leads to the separation of particles and the increase of the void fraction in emulsion phase [11]. As a result, the average size of bubbles shrank and the rise velocity of bubbles decreased. Secondly, when particles are charged, the minimum fluidization velocity becomes greater than that of

uncharged particles [32]. As the superficial gas velocity remains unchanged, the volume of gas to form bubbles ($u-u_{mf}$) decreased and the average size of bubbles reduced. Since rising bubbles are the driving force of particle motions, the intensity of particle motions was inhibited.

3.2 Online measurement of particle charge-to-mass ratio

Based on previous research [33], it can be inferred that the relation among induced electrostatic voltage, particle charge-to-mass ratio and particle velocity could be illustrated by Eq. (2).

$$V_{ind} = K_e \cdot v_c^a \cdot q_m^b \quad (2)$$

where V_{ind} represents the average positive induced electrostatic voltage (V), v_c stands for the average correlation velocity of charged particles (m/s), q_m is the average particles charge-to-mass ratio ($\mu\text{C}/\text{kg}$), and K_e is the proportion factor which is related to the meter factor (K) of correlation velocity [22], the amplification factor of the electrostatic circuit and the particle concentration distribution, etc. Eq. (3) can be obtained by natural logarithm processing of Eq. (2),

$$\ln V_{ind} = a \ln v_c + b \ln |q_m| + \ln K_e \quad (3)$$

Since q_m could be negative in the experimental system, the absolute value of q_m was used in Eq. (3) in the regression process. In Section 3.1, the average positive electrostatic voltage, the average correlation velocity and the average particles charge-to-mass ratio have been obtained under different charging levels. Data displayed in Table 5 was used to regress the coefficients in Eq. (3) by the least square method.

Based on the data shown in Table 5, Eq. (4) was regressed to indicate how the average correlation velocity and the average particles charge-to-mass ratio affected the induced electrostatic voltage. The R-squared of the regression was 0.959.

$$V_{ind} = 0.41v_c^{1.1} |q_m|^{0.485} \quad (4)$$

From Eq. (4), it can be inferred that the induced electrostatic voltage signals were more sensitive to the variation of particle velocity, which was in accordance with the experimental results above. For example, when fresh particles were fluidized for a short time, the electrostatic charges accumulation on particles was not obvious, and the particle velocity was relatively great since it had not been affected by charges accumulation. During this period, only evident electrostatic voltage signals could be detected. Besides, when enough LAA was injected into the fluidized bed to control the average particles charge-to-mass ratio to nearly zero, the particle motions were vigorous and the average correlation velocity of particle clouds reached maximum. At this time, the electrostatic voltage signals could also be measured and used for cross-correlation calculation. On the basis of Eq. (4), the average particles charge-to-mass ratio can be calculated by measuring induced electrostatic voltage signals and the average correlation velocity of particle clouds.

Figure 13 compares the average particles charge-to-mass ratios obtained by Eq. (4) and offline Faraday cup sampling method. It can be found that at two axial heights, the average particles charge-to-mass ratios estimated by Eq. (4) showed the same variation tendency as those measured by Faraday cup with increasing gas velocity. When the excess gas velocity was 0.3 m/s or 0.4 m/s, the relative error of estimated values was within 10% compared with results from Faraday cup. When the excess gas velocity was 0.2 m/s or 0.5 m/s, the relative error increased but still remained no more than 40%. It could be found that when the excess gas velocity was close to the excess velocity shown in Table 5, the accuracy of the estimated results was better. When the gas velocity was far away from the basic data used for model regression, the accuracy of the estimation reduced, but still showed the same trend with that of Faraday cup. This means that although the prediction model of particle charge-to-mass ratio was regressed based on the data obtained under a certain gas velocity, it can be applied to the estimation of q_m in the fluidized beds within a range of gas velocities.

The distinction between the results from Eq. (3) and Faraday cup could be

caused by the following reasons. Firstly, during the regression and estimation process, K_e was supposed to be a constant under various gas velocities. However, K_e can be affected by the particle velocity and concentration distributions, which were not concerned in this work. Since K_e should be different under various gas velocities, this may cause an error of the estimated results. Secondly, the sampling process of Faraday cup method would affect the charges carried by particles to a certain extent, which brought in an error to the measured results by Faraday cup. Besides, sampled particles measured by Faraday cup were mainly from the region near the wall of the fluidized bed. While for the electrostatic voltage signals measured by arc-shaped sensors, they were affected by all the charged particles in the cross section of the fluidized bed. For these two methods, the measured particles came from different local regions of the fluidized bed. As a result, a discrepancy existed between the results from these two methods.

Since both the induced electrostatic voltage signals and the correlation velocity of particles come from the arc-shaped induced electrostatic sensors array combined with cross-correlation method, an online method to measure particles charge-to-mass ratios has been established based on the arc-shaped induced electrostatic sensors array in the gas-solid fluidized bed. The predictive model in this work can be applied to the estimation of average particles charge-to-mass ratios in the bubbling regime with PE particles and Plexiglas fluidized bed.

4. Conclusions

This work investigated the effect of electrostatic charges accumulation on particle motions by injecting a trace of LAA to the fluidized bed. A predictive model of particles charge-to-mass ratio was established to complement the online measurement of particles charge-to-mass ratios by arc-shaped induced electrostatic sensors array.

It was found that the change of electrostatic charge level had nearly no effect on

the correlation between the upstream and downstream electrostatic voltage signals. This ensured that the correlation velocity of particles could be used to characterize the intensity of particle motions whether the particles were charged to a saturate level or not.

With the increase of LAA content, the average correlation velocities of Geldart D and B particles increased and the normalized probability distribution of correlation velocities broadened. When the excess gas velocity was 0.35 m/s and particles were charged to a saturate level, the average correlation velocities of Geldart D and B particles decreased by 26% and 50%, respectively, compared with those the results when the particles were nearly uncharged. It was demonstrated that electrostatic charges accumulation would restrain particle motions inside the fluidized bed.

Based on the induced electrostatic voltage signals, the average correlation velocities of particles and the average particles charge-to-mass ratios under different electrostatic charge levels, a predictive model was established to estimate the average particles charge-to-mass ratios in the fluidized beds. The estimated results showed the same tendency as the results measured by Faraday cup with the increase of gas velocity. The relative error was no more than 40%. Therefore, it is promising that the average particles charge-to-mass ratio and correlation velocity could be measured simultaneously online by arc-shaped induced electrostatic sensors array in the gas-solid fluidized bed.

Notations

a	constant in the predictive model of average particles charge-to-mass ratio, dimensionless
b	constant in the predictive model of average particles charge-to-mass ratio, dimensionless
H	axial distance from the distributor, mm
K	meter factor of correlation velocity, dimensionless
K_e	constant in the predictive model of average particles charge-to-mass ratio
q_m	average particles charge-to-mass ratio, $\mu\text{C}/\text{kg}$
u	superficial gas velocity, m/s
u_e	excess gas velocity, m/s

- u_{mf} minimum fluidization velocity, m/s
 V_{ind} average of positive induced electrostatic voltage, V
 v_c average correlation velocity of particle clouds, m/s

Acknowledgements

The authors are grateful for the financial support of this work by the National Natural Science Foundation of China (No. 21236007), the National Science Fund for Distinguished Young (21525627), the National Natural Science Foundation of China (No. 61403138), the Natural Science Foundation of Zhejiang Province (Grant No. LR14B060001) and the Specialized Research Fund for the Doctoral Program of Higher Education (Grant 20130101110063).

References

- [1] M. Stein, Y.L. Ding, J.P.K. Seville, D.J. Parker, Solids motion in bubbling gas fluidised beds, *Chemical Engineering Science*, 55 (2000) 5291-5300.
- [2] X. Fan, Z. Yang, D.J. Parker, B. Armstrong, Prediction of bubble behaviour in fluidised beds based on solid motion and flow structure, *Chemical Engineering Journal*, 140 (2008) 358-369.
- [3] G. Hendrickson, Electrostatics and gas phase fluidized bed polymerization reactor wall sheeting, *Chemical Engineering Science*, 61 (2006) 1041-1064.
- [4] Y. Cheng, E.W.C. Lim, C.H. Wang, G. Guan, C. Fushimi, M. Ishizuka, A. Tsutsumi, Electrostatic characteristics in a large-scale triple-bed circulating fluidized bed system for coal gasification, *Chemical Engineering Science*, 75 (2012) 435-444.
- [5] M.A. Hassani, R. Zarghami, H.R. Norouzi, N. Mostoufi, Numerical investigation of effect of electrostatic forces on the hydrodynamics of gas-solid fluidized beds, *Powder Technology*, 246 (2013) 16-25.
- [6] D. Boland, D. Geldart, Electrostatic charging in gas fluidized beds, *Powder Technology*, 5 (1972) 289-297.
- [7] J. Guardiola, V. Rojo, G. Ramos, Influence of particle size, fluidization velocity and relative humidity on fluidized bed electrostatics, *Journal of Electrostatics*, 37 (1996) 1-20.
- [8] A. Giffin, P. Mehrani, Effect of gas relative humidity on reactor wall fouling generated due to bed electrification in gas-solid fluidized beds, *Powder Technology*, 235 (2013) 368-375.
- [9] Y. Zhou, C. Ren, J. Wang, Y. Yang, K. Dong, Effect of hydrodynamic behavior on electrostatic potential distribution in gas-solid fluidized bed, *Powder Technology*, 235 (2013) 9-17.
- [10] J. Lowell, W.S. Truscott, Triboelectrification of identical insulators. II. Theory and further experiments, *Journal of Physics D: Applied Physics*, 19 (1986) 1281.
- [11] K. Dong, Q. Zhang, Z. Huang, Z. Liao, J. Wang, Y. Yang, Experimental investigation of electrostatic effect on bubble behaviors in gas-solid fluidized bed, *AIChE Journal*, 61 (2015) 1160-1171.
- [12] K. Dong, Q. Zhang, Z. Huang, Z. Liao, J. Wang, Y. Yang, F. Wang, Experimental investigation of electrostatic effect on particle motions in gas-solid fluidized beds, *AIChE Journal*, 61 (2015) 3628-3638.
- [13] F. Jalalinejad, X.T. Bi, J.R. Grace, Effect of electrostatics on freely-bubbling beds of mono-sized particles, *International Journal of Multiphase Flow*, 70 (2015) 104-112.
- [14] F. Wang, J.D. Wang, Y.R. Yang, Distribution of electrostatic potential in a gas-solid fluidized bed and measurement of bed level, *Industrial & Engineering Chemistry Research*, 47 (2008) 9517-9526.
- [15] J. Wang, Y. Xu, W. Li, Y. Yang, F. Wang, Electrostatic potentials in gas-solid fluidized beds influenced by the injection of charge inducing agents, *Journal of Electrostatics*, 67 (2009) 815-826.
- [16] P. Tiyapiboonchaiya, D. Gidaspow, S. Damronglerd, Hydrodynamics of electrostatic charge in polypropylene fluidized beds, *Industrial & Engineering Chemistry Research*, 51 (2012) 8661-8668.
- [17] C. He, X.T. Bi, J.R. Grace, Contact electrification of a novel dual-material probe with charged particulate flow, *Powder Technology*, 253 (2014) 1-9.
- [18] C. He, X.T. Bi, J.R. Grace, Simultaneous measurements of particle charge density and bubble properties in gas-solid fluidized beds by dual-tip electrostatic probes, *Chemical Engineering Science*,

123 (2015) 11-21.

- [19] C. He, X.T. Bi, J.R. Grace, Comparison of conventional and novel probes for measuring electrostatics and hydrodynamics during fluidization of polyethylene, *Journal of Electrostatics*, 79 (2016) 7-15.
- [20] C.L. Xu, C. Liang, B. Zhou, S.M. Wang, HHT analysis of electrostatic fluctuation signals in dense-phase pneumatic conveying of pulverized coal at high pressure, *Chemical Engineering Science*, 65 (2010) 1334-1344.
- [21] C.L. Xu, B. Zhou, S.M. Wang, Dense-phase pneumatically conveyed coal particle velocity measurement using electrostatic probes, *Journal of Electrostatics*, 68 (2010) 64-72.
- [22] Y. Yan, B. Byrne, S. Woodhead, J. Coulthard, Velocity measurement of pneumatically conveyed solids using electrodynamic sensors, *Meas. Sci. Technol.*, 6 (1995) 515-537.
- [23] Y. Yan, Mass flow measurement of bulk solids in pneumatic pipelines, *Meas. Sci. Technol.*, 7 (1996) 1687-1706.
- [24] W.B. Zhang, C. Wang, Y.L. Wang, Parameter selection in cross-correlation based velocimetry using circular electrostatic sensors, *Ieee Transactions on Instrumentation and Measurement*, 59 (2010) 1268-1275.
- [25] W.B. Zhang, Y.P. Cheng, C. Wang, W.Q. Yang, C.H. Wang, Investigation on hydrodynamics of triple-bed combined circulating fluidized bed using electrostatic sensor and electrical capacitance tomography, *Industrial & Engineering Chemistry Research*, 52 (2013) 11198-11207.
- [26] W. Zhang, Y. Yan, Y. Yang, J. Wang, Measurement of Flow Characteristics in a Bubbling Fluidized Bed Using Electrostatic Sensor Arrays, *IEEE Transactions on Instrumentation and Measurement*, 65 (2016) 703-712.
- [27] A.H. Chen, H. Bi, J.R. Grace, Effects of charge distribution around bubbles on charge induction and transfer to a ball probe in gas-solid fluidized beds, *Journal of Electrostatics*, 58 (2003) 91-115.
- [28] A.H. Chen, H.T. Bi, J.R. Grace, Measurement of particle charge-to-mass ratios in a gas-solids fluidized bed by a collision probe, *Powder Technology*, 135 (2003) 181-191.
- [29] C. He, X.T. Bi, J.R. Grace, Decoupling electrostatic signals from gas-solid bubbling fluidized beds, *Powder Technology*, 290 (2016) 11-20.
- [30] K. Daizo, O. Levenspiel, *Fluidization Engineering*, Butterworth, Boston, 1991.
- [31] D. Geldart, Types of Gas Fluidization, *Powder Technology*, 7 (1973) 285-292.
- [32] K. Dong, Electrostatic influence on hydrodynamics and charge control investigation in gas-solid fluidized bed, *Chemical and Biological Engineering*, Zhejiang University, Hangzhou, 2015.
- [33] Q. Zhang, K. Dong, Y. F. Zhou, Z. L. Huang, Z. W. Liao, J. D. Wang, Y. R. Yang, F. Wang. A comparative study of electrostatic current and pressure signals in a MSFC gas-solid fluidized bed. *Powder Technology*, 287 (2016) 292-300.

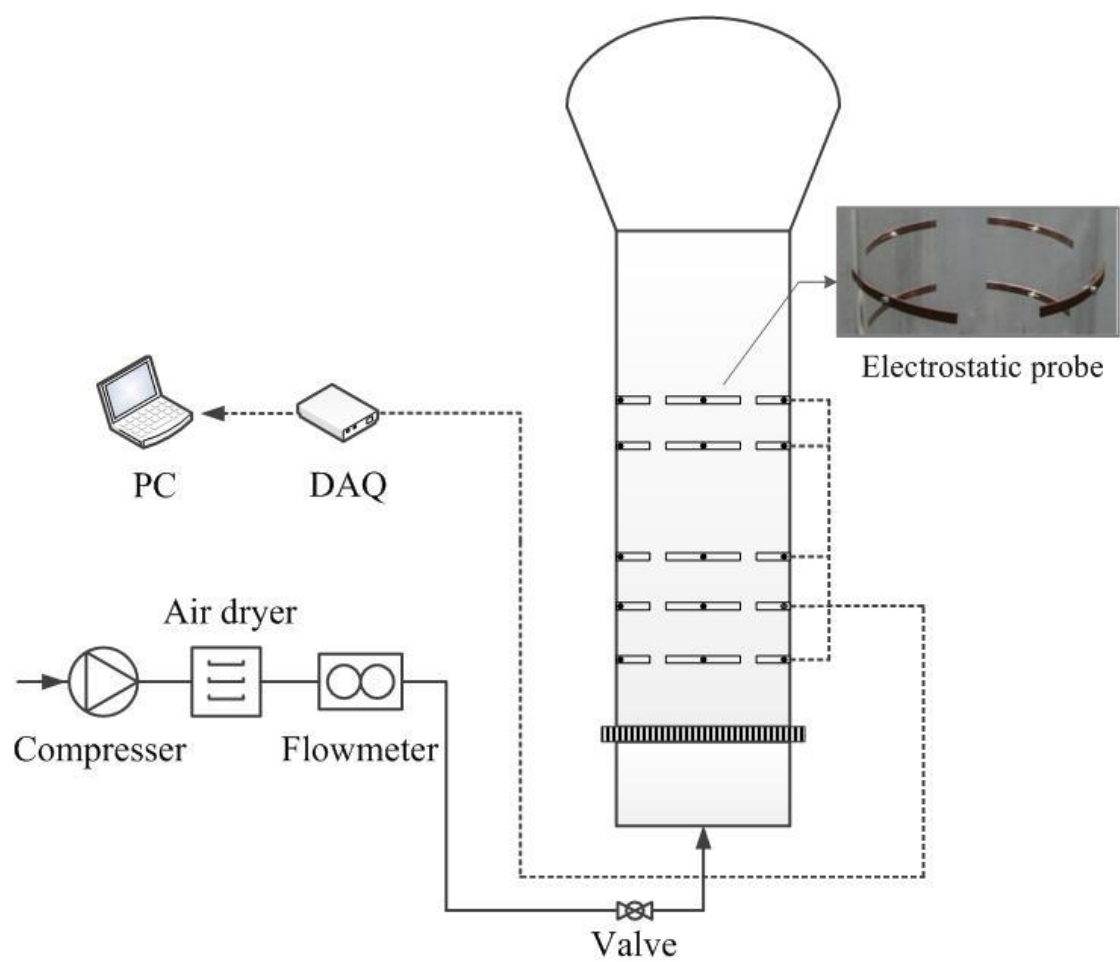


Fig. 1

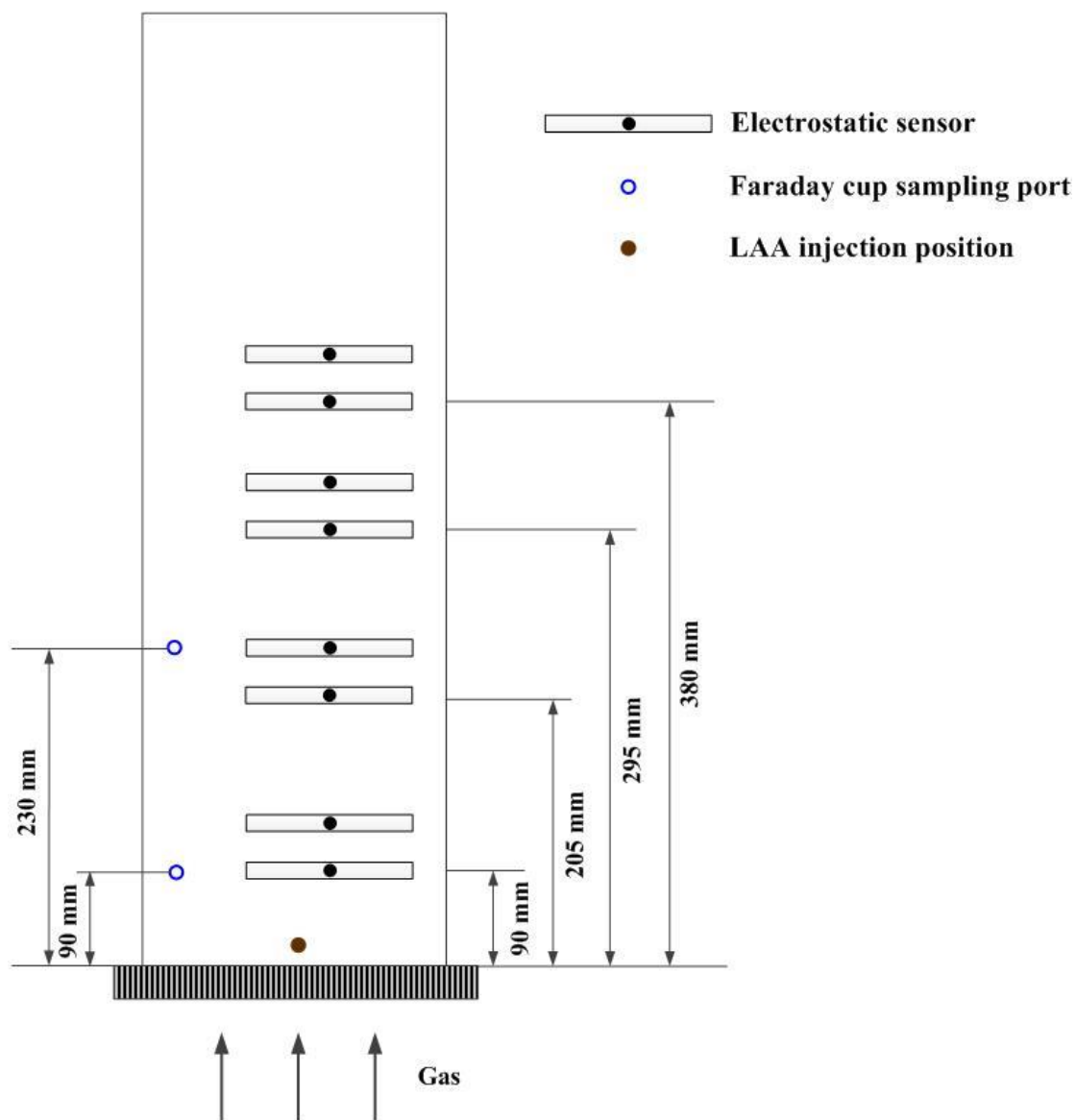


Fig. 2

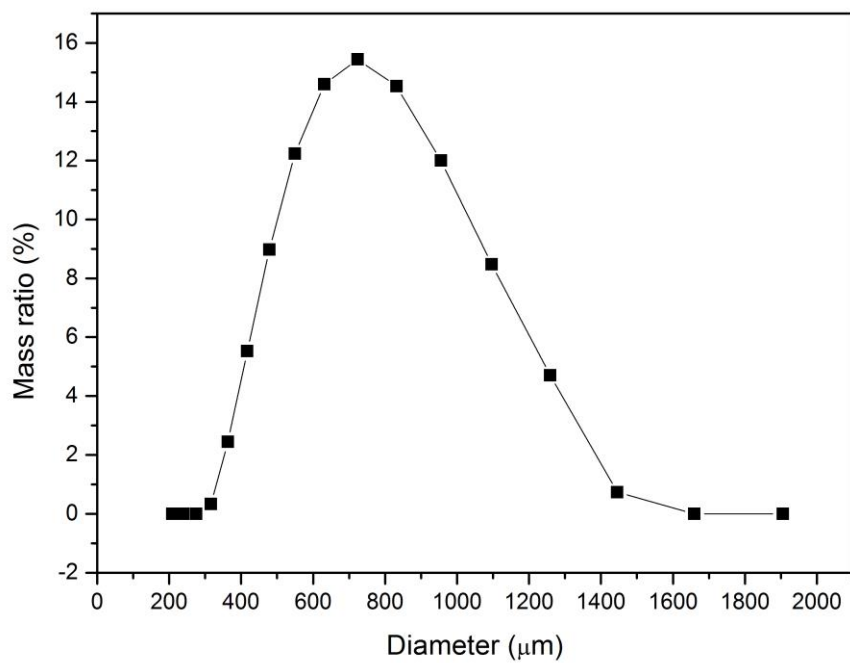


Fig. 3

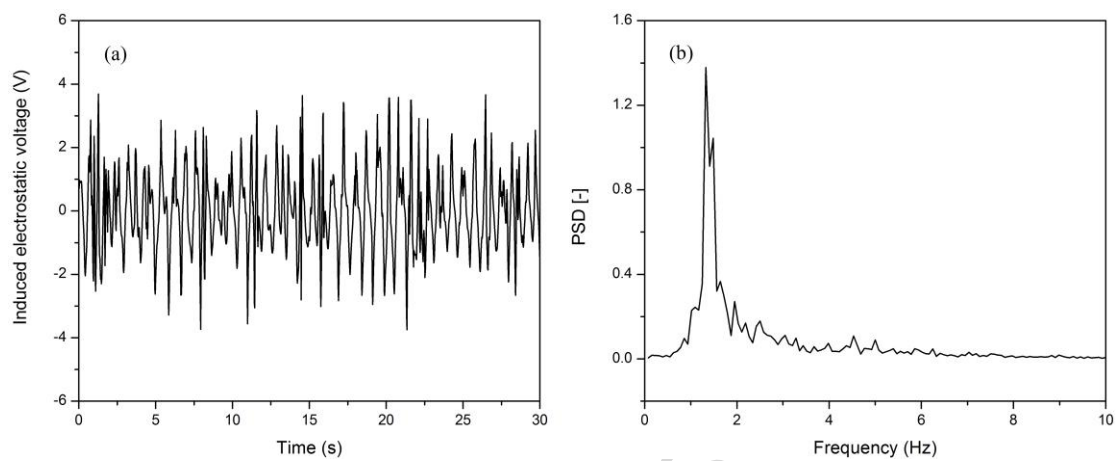


Fig. 4

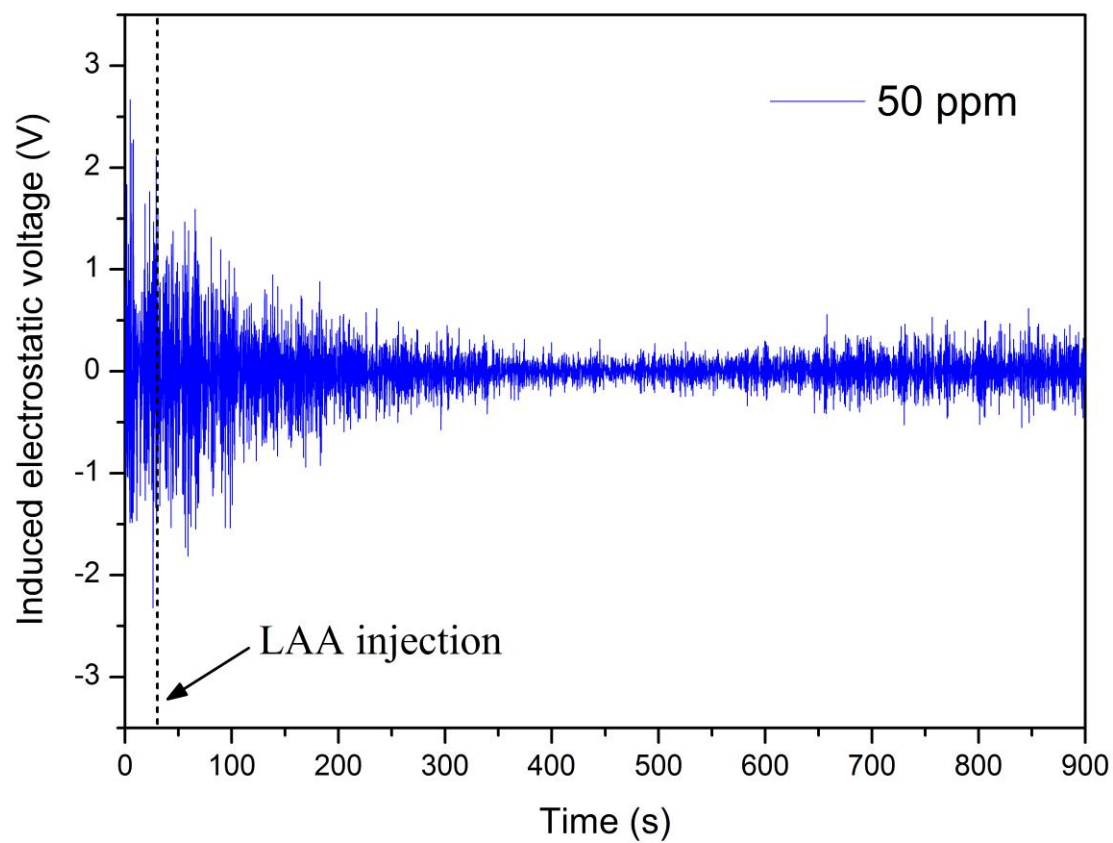


Fig. 5

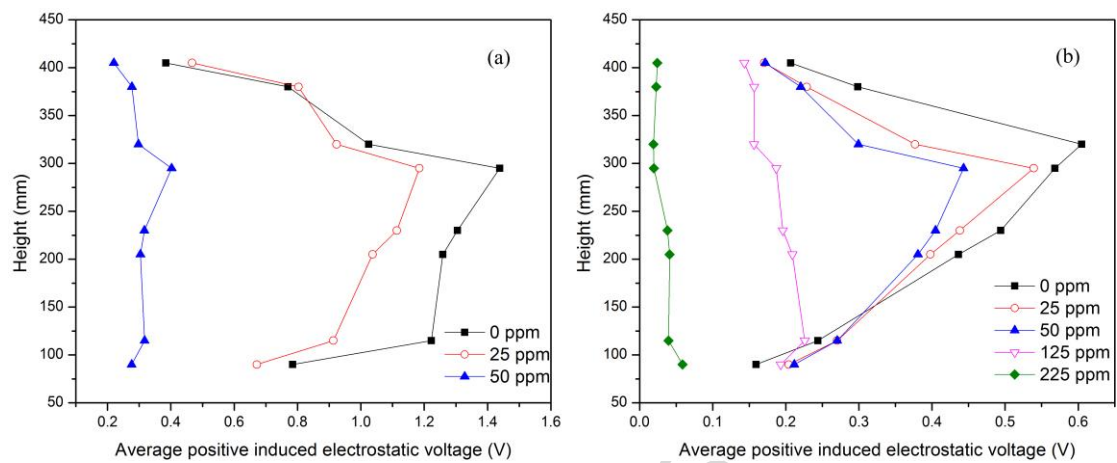


Fig. 6

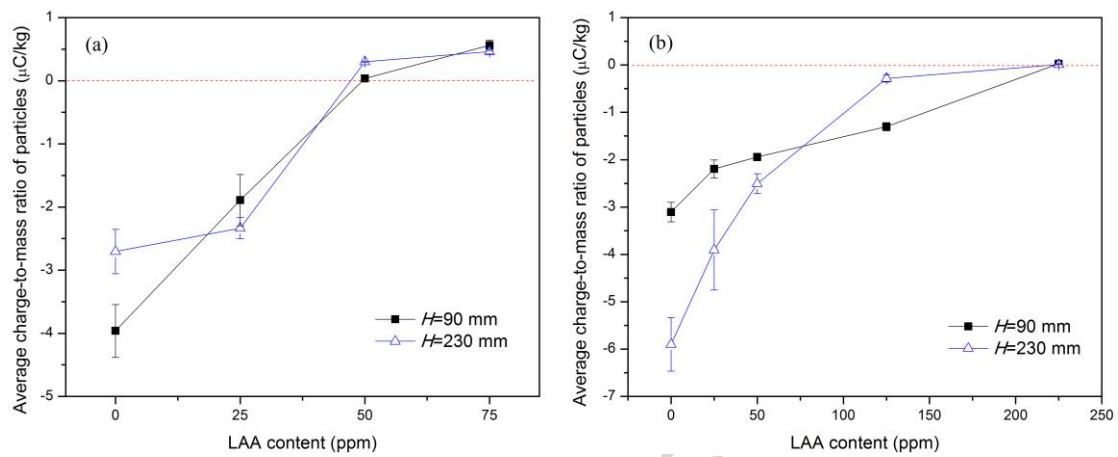


Fig. 7

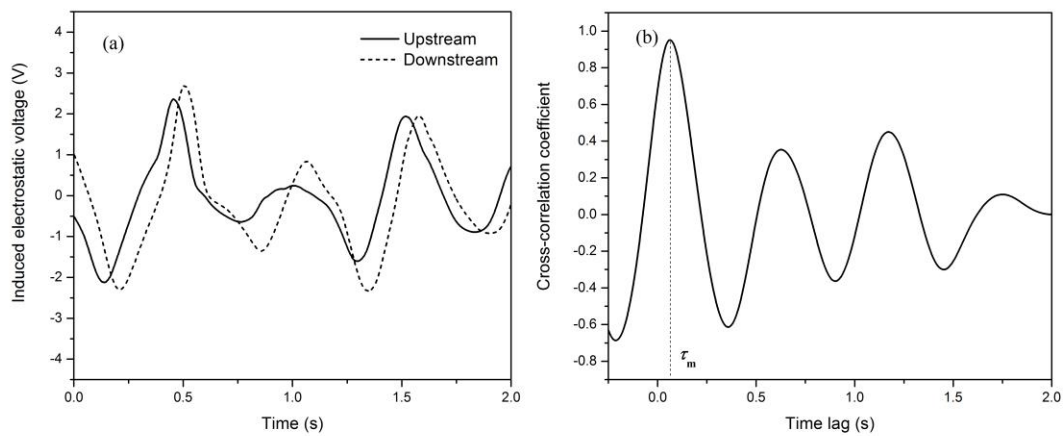


Fig. 8

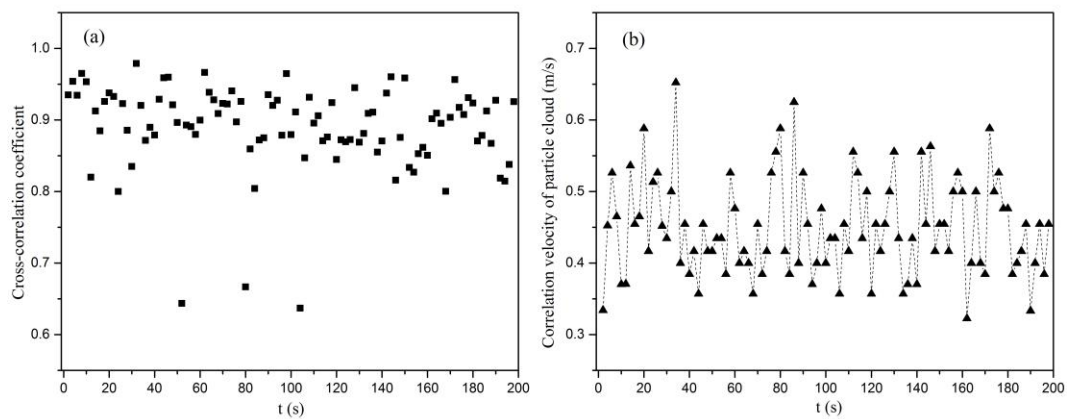


Fig. 9

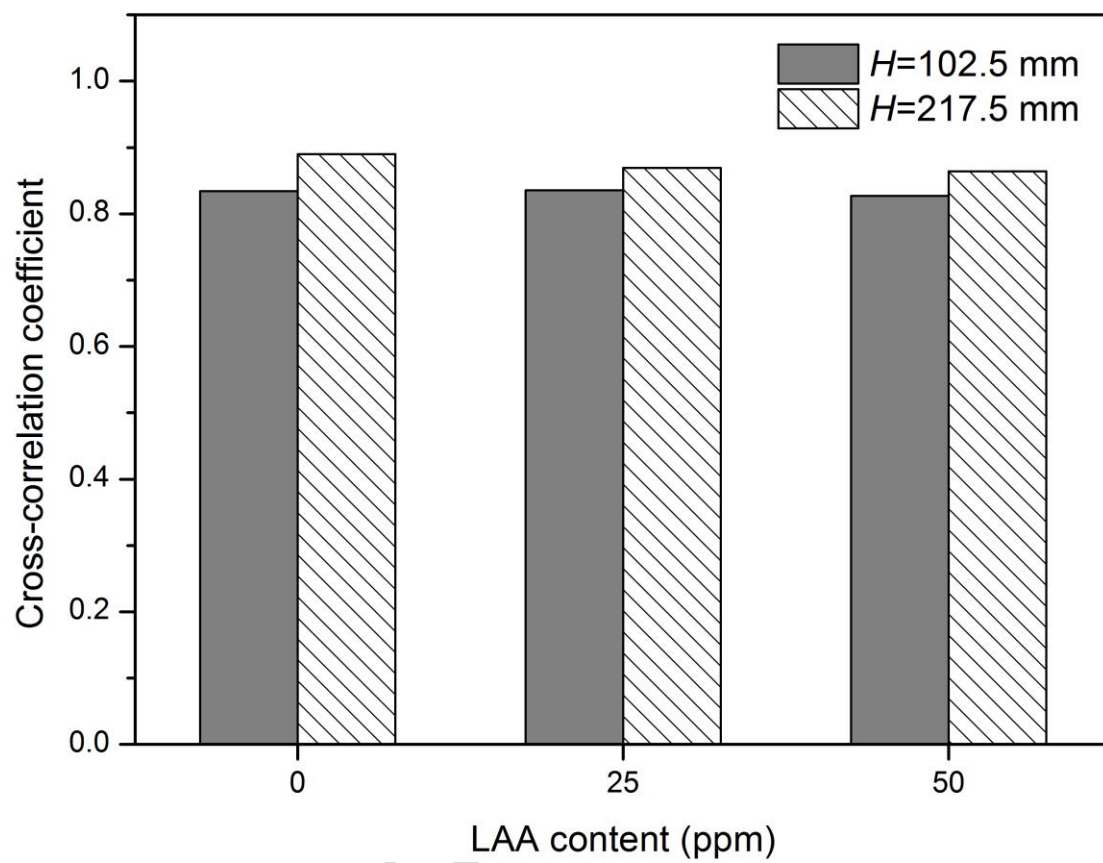


Fig. 10

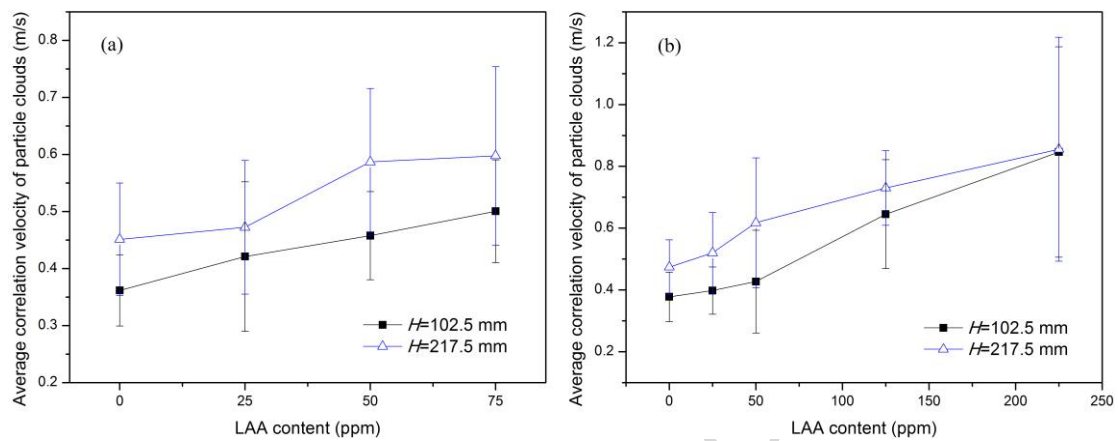


Fig. 11

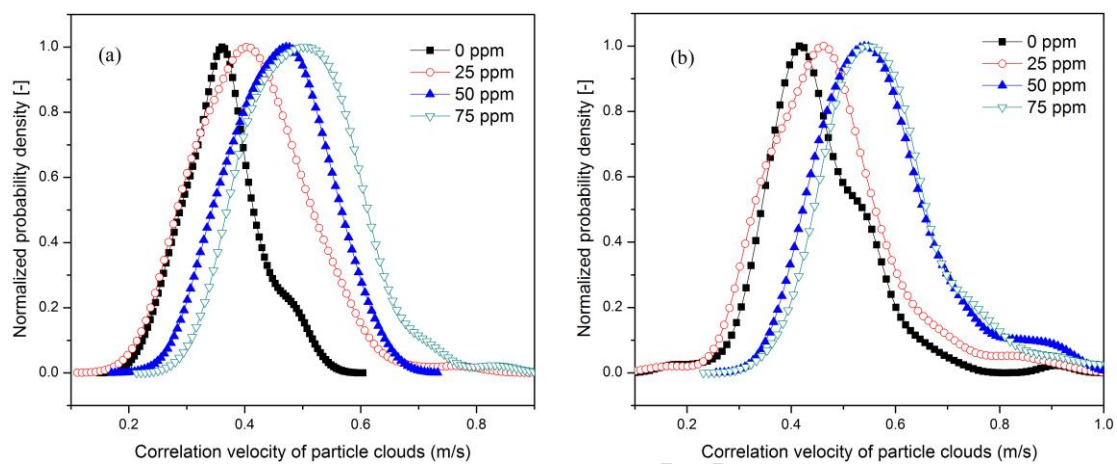


Fig. 12

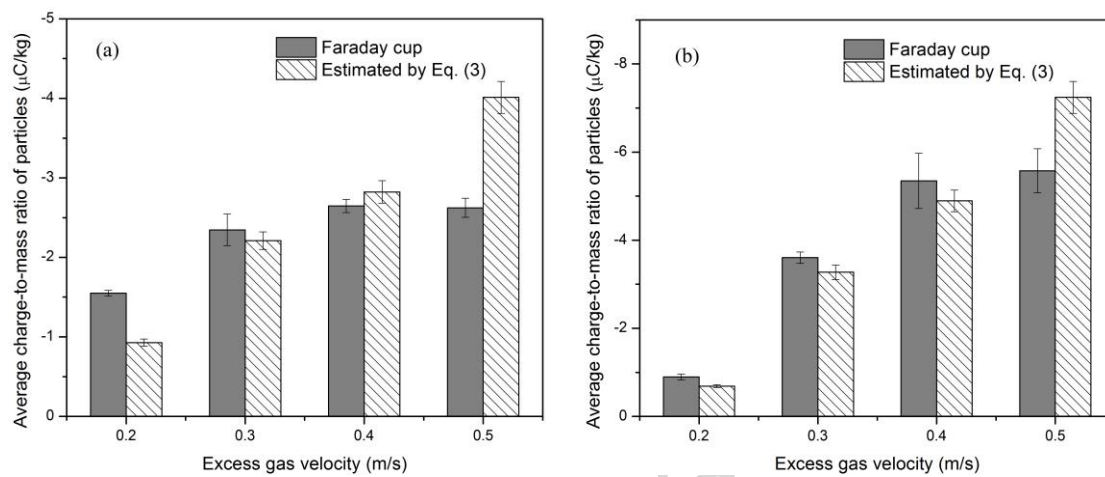


Fig. 13

Figure 1. Schematic diagram of the experimental apparatus.

Figure 2. Layout of arc-shaped electrostatic sensors' installation and positions for particles sampling and LAA injection.

Figure 3. Particle size distribution of linear low density polyethylene (LLDPE) particles.

Figure 4. Induced electrostatic voltage signals variation with time and the corresponding PSD.

Figure 5. Variation of induced electrostatic voltage with time after injection of LAA ($u_e=0.35$ m/s, $H=180$ mm, Geldart D particles).

Figure 6. Variations of axial profiles of average positive induced electrostatic voltage with LAA contents ($u_e=0.35$ m/s). (a) Geldart D particles, (b) Geldart B particles

Figure 7. Variations of average charge-to-mass ratios of particles with LAA contents ($u_e=0.35$ m/s). (a) Geldart D particles, (b) Geldart B particles

Figure 8. Induced electrostatic voltage signals from upstream and downstream sensors and the corresponding cross-correlation function ($u_e=0.35$ m/s, Geldart D particles, $H=217.5$ mm, LAA contents 25 ppm). (a) Induced electrostatic voltage with time, (b) Cross-correlation function

Figure 9. Cross-correlation coefficients of electrostatic voltage signals from upstream and downstream sensors and their corresponding correlation velocities ($u_e=0.35$ m/s, Geldart D particles, $H=217.5$ mm, LAA contents 25 ppm). (a) Cross-correlation coefficient, (b) Correlation velocities of particle cloud

Figure 10. Variations of average cross-correlation coefficient for upstream and downstream electrostatic voltage signals with LAA contents. ($u_e=0.35$ m/s, Geldart D particles)

Figure 11. Variations of average correlation velocity at two axial heights with LAA content ($u_e=0.35$ m/s). (a) Geldart D particles, (b) Geldart B particles

Figure 12. Variations of normalized probability density distributions of average correlation velocities with LAA contents at two axial heights ($u_e=0.35$ m/s). (a) $H=102.5$ mm, (b) $H=217.5$ mm

Figure 13. Comparisons of average particle charge-to-mass ratios obtained by Eq. (3) and Faraday cup under different excess gas velocities (Geldart B particles). (a) $H=102.5$ mm, (b) $H=217.5$ mm

Table 1. Physical properties of particles and specific operating parameters in this work.

Materials	Density (kg/m ³)	Diameter (mm)	Geldart type [31]	u_{mf} (m/s)	u (m/s)
LLDPE	918	0.45-0.90	B	0.20	0.35,0.4,0.5,0.55,0.6,0.7
PP	900	~1.85	D	0.55	0.7,0.8,0.9,1.0

Table 2. LAA injection content for LLDPE particles (1.5 kg).

Mass ratio (ppm)	25	50	75	125	225
Volume (mL)	0.045	0.090	0.135	0.225	0.405

Table 3. LAA injection content for PP particles (2.0 kg).

Mass ratio (ppm)	25	50	75	100
Volume (mL)	0.060	0.120	0.180	0.240

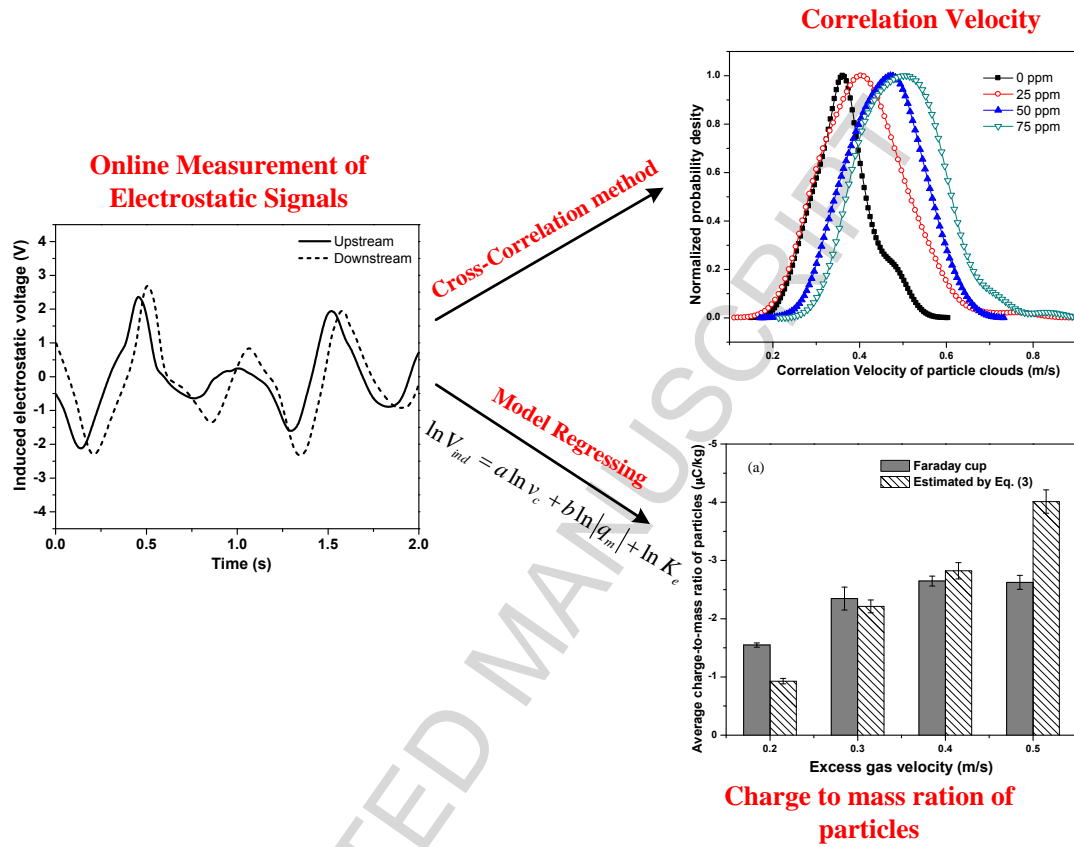
Table 4. Average correlation velocities of particle clouds under different excess gas velocities with and without electrostatic charges at two axial heights.

Position	u_e (m/s)	v_c of Geldart D particles (m/s)		v_c of Geldart B particles (m/s)	
		Charged	Uncharged	Charged	Uncharged
$H=217.5$ mm	0.15	0.356	0.534	0.406	0.565
$H=102.5$ mm	0.15	0.206	0.382	0.277	0.451
$H=217.5$ mm	0.35	0.451	0.598	0.474	0.855
$H=102.5$ mm	0.35	0.365	0.500	0.377	0.846

Table 5. Data for coefficients regression of Geldart B particles.

LAA content (ppm)	$H=102.5$ mm			$H=217.5$ mm		
	V_{ind} (V)	v_c (m/s)	q_m (μ C/kg)	V_{ind} (V)	v_c (m/s)	q_m (μ C/kg)
0	0.2016	0.378	-3.107	0.4651	0.474	-5.899
25	0.2371	0.398	-2.196	0.4180	0.520	-3.907
50	0.2409	0.427	-1.944	0.3928	0.617	-2.507
125	0.2094	0.645	-1.303	0.2024	0.730	-0.2834
225	0.04919	0.846	0.02580	0.03969	0.855	0.0098

Graphic Abstract for review:



Highlights:

- * Induced electrostatic signals and particle correlation velocity were measured.
- * Electrostatic charges accumulation restrained the particle motions.
- * A mathematical model was established to predict the particles charge-to-mass ratio.

ACCEPTED MANUSCRIPT